Computational Study of Structural, Electronic, and Optical Properties of Crystalline NH4N3

3 AUTHORS:

Yedukondalu Neelam
University of Hyderabad
15 PUBLICATIONS **39** CITATIONS

SEE PROFILE

Vikas D. Ghule
National Institute of Technology, Kurukshetra
36 PUBLICATIONS **252** CITATIONS

SEE PROFILE

Ganapathy Vaitheeswaran
University of Hyderabad
118 PUBLICATIONS **1,348** CITATIONS

SEE PROFILE

Computational Study of Structural, Electronic, and Optical Properties of Crystalline NH$_4$N$_3$

N. Yedukondalu, Vikas D. Ghule, and G. Vaitheeswaran*

Advanced Centre of Research in High Energy Materials (ACRHEM), University of Hyderabad, Prof. C. R. Rao Road, Gachibowli, Andhra Pradesh, Hyderabad 500 046, India

ABSTRACT: A systematic computational study on the structural, electronic, bonding, and optical properties of orthorhombic ammonium azide (NH$_4$N$_3$) has been performed using planewave pseudopotential (PW-PP) method based on density functional theory (DFT). Semiempirical dispersion correction schemes have been used to account for nonbonded interactions in molecular crystalline NH$_4$N$_3$. The ground state lattice parameters, and fractional coordinates obtained using the dispersion correction schemes are in excellent agreement with experimental results. We calculated the single crystal elastic constants of NH$_4$N$_3$, and its sensitivity is interpreted through the observed ordering of the elastic constants ($C_{33} > C_{11} > C_{22}$). The electronic structure and optical properties were calculated using full potential linearized augmented plane wave (FP-LAPW) approach with recently developed functional of Tran–Blaha modified Becke–Johnson (TB-mBJ) potential. The TB-mBJ electronic structure shows that NH$_4$N$_3$ is a direct band gap insulator with a band gap of 5.08 eV, while the calculated band gap with standard generalized gradient approximation is found to be 4.10 eV. The optical anisotropy is analyzed through the calculated optical constants, namely, dielectric function and refractive index along three different crystallographic axes. The absorption spectra reveal that NH$_4$N$_3$ is sensitive to ultraviolet (UV) light. Further, we also analyzed the detonation characteristics of the NH$_4$N$_3$ using the reported heat of formation and calculated density. NH$_4$N$_3$ is found to have a detonation velocity of 6.45 km/s and a detonation pressure about 15.16 GPa computed by Kamlet–Jacobs empirical equations.
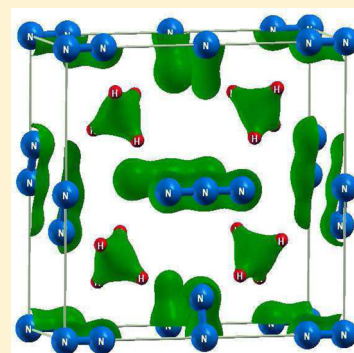
1. INTRODUCTION

NH$_4$N$_3$ belongs to the class of inorganic azides, which are an interesting group of materials with a wide range of applications as explosives and photographic materials. They served as model systems for studying the fast reactions in crystalline solids with complex chemical bonding.[1,2] Alkali metal azides in particular sodium azide can be used to synthesize polymeric nitrogen under extreme conditions, which is a green high energy density material (HEDM),[3,4] and it can be used as rocket fuel or propellant.[5] Among the inorganic azides, NH$_4$N$_3$ is of special interest due to the strong hydrogen bonding features between the ammonium cation and the negatively charged azide anion, which can be considered as a model hydrogen-bonded system.[6–8] NH$_4$N$_3$, first obtained by Curtius,[9] is a highly potential azide for its ability to detonate powerfully with a very low sensitivity. NH$_4$N$_3$ is thermally unstable inorganic azide, which is highly volatile and undergoes molecular sublimation. Recently, Eslami et al.[10] reported the microencapsulation techniques to stabilize volatile NH$_4$N$_3$, while Ng et al.[11] made an early comprehensive experimental analysis of NH$_4$N$_3$ based on the sublimation kinetics over the temperature range 360–389 K. The reported differential scanning calorimetry thermogram results confirm the endothermic (73.4 kJ/mol) nature of NH$_4$N$_3$, and its vapor readily dissociates into ammonia and hydrazoic acid.[11,12]

Materials that contain hydrogen and nitrogen alone are considered to be promising candidates for HEDMs as their decomposition reactions give environmental friendly gases such as nitrogen and hydrogen. The high volatile nature, thermal instability, and impact sensitivity of NH$_4$N$_3$ are the main disadvantages for its usage in energetic material formulations. However, NH$_4$N$_3$ is capable of considerable brisance[13] owing to the rapid evolution of gaseous products. Apart from its usage as a weak explosive, its potential as a gas generator has received much attention in recent years. NH$_4$N$_3$ has been used to inflate safety cushions in automobiles with a suitable oxidizer[14] and also used as a solid propellant in photochemical microrockets for altitude control.[15] NH$_4$N$_3$ is a derivative of nitric-hydro-acids, which is an important component of rocket fuels.[16] Moreover, recent experiments[6,7] reveal that NH$_4$N$_3$ undergoes a polymorphic phase transition about 3 GPa due to modification in the strength of hydrogen bonding, and also, the high pressure phase is thermodynamically stable up to 55 GPa, while ab initio studies predict the high pressure phase of NH$_4$N$_3$ to nonmolecular hydro-nitrogen solid at 36 GPa, which is a HEDM with wide range of applications.[17]

Over the past several decades, a number of studies have been devoted to the structural properties and decomposition mechanism of NH$_4$N$_3$.[11,18,19] However, many fundamental aspects of NH$_4$N$_3$ are still not well understood because of its complex chemical behavior. The detailed knowledge about the crystal structure of azides is very important in order to

understand the stability and decomposition. One of the primary objectives of this study is to understand ground state electronic structure and optical properties of NH_4N_3, which are not investigated so far at the ab initio level.

The rest of the article is organized as follows: in section II, we briefly describe the computational details. Results and discussion concerning structural and elastic properties of NH_4N_3 are presented in section 3.1, sections 3.2 and 3.3 contain the details of electronic structure, bonding, and optical properties of NH_4N_3. In section 3.4, we discuss the detonation characteristics of NH_4N_3, and finally, section 4 summarizes the conclusions.

2. COMPUTATIONAL DETAILS

First-principles calculations were performed by using two distinct approaches known as PW-PP and FP-LAPW methods. Structural and elastic properties were obtained using the PW-PP approach as implemented in Cambridge Series of Total Energy Package[20−22] based on DFT.[23,24] We used Vanderbilt-type[25] ultrasoft pseudopotentials for electron−ion interactions. The local density approximation (LDA)[26,27] and generalized gradient approximation (GGA)[28] were used to treat electron−electron interactions in NH_4N_3. The standard LDA (CA-PZ) and GGA (PBE) functionals are inadequate to predict the long-range interactions in molecular crystalline solids.[29−31] However, the noncovalent interactions such as hydrogen bonding and van der Waals interactions play a key role in determining the physical and chemical properties of molecular solids. Hence, the semiempirical approaches have been developed in order to account for the long-range interactions in the molecular solids, and they were incorporated through standard DFT description. In the present study, we have used two dispersion correction schemes. First, G06 scheme by Grimme,[32] which is an empirical correction to DFT taking into account of the dispersive interactions based on damped and atomic pairwise potentials of the form $C_6 \cdot R^{-6}$. Second, TS scheme recently developed by Tkatchenko and Scheffler[33] based on the summation of interatomic C_6 coefficients derived from the electron density of molecule or solid and accurate data for the free atoms. The C_6 coefficients used in the calculations, for N and H atoms, are 12.75 and 1.451 in G06 and 14.46 and 3.884 eV·Å^6 in TS schemes, respectively. We systematically studied the effect of semiempirical dispersion correction schemes on the structural properties of the NH_4N_3 along with standard DFT functionals and discuss the same in detail in the following section. The Broyden−Fletcher−Goldfarb−Shanno (BFGS) minimization scheme[34] has been used for structural relaxation. The plane wave basis orbitals used in the calculations are $2s^2$, $2p^3$ for N and $1s^1$ for H. The convergence criteria for structural optimization was set to fine quality with a kinetic energy cutoff of 580 eV and k-mesh 4 × 6 × 4 according to the Monkhorst−Pack grid scheme.[35] The self-consistent energy convergence was set to 1.0×10^{-5} eV/atom. The convergence criterion for the maximal force between atoms was 0.03 eV/A. The maximum displacement and stress were set to be 1.0×10^{-2} Å and 0.05 GPa, respectively.

It is well-known that the standard DFT functionals LDA and GGA usually underestimate the energy band gap about 50% when compared to experiments. The LDA and GGA functionals suffer from artificial electron self-interaction and also lack the derivative discontinuities of the exchange-correlation potential with respect to occupation number.[36] The calculation of band gap involves only exchange energy,[37]

and it was determined very accurately by the TB-mBJ functional[38] when compared to standard DFT functionals. Hence, this semilocal functional provides much improved band gaps for semiconductors and insulators. Therefore, the electronic structure and optical properties of NH_4N_3 were calculated by using this TB-mBJ functional as implemented in the WIEN2k package.[39] To achieve energy eigen value convergence, wave functions in the interstitial region were expanded in plane waves with cutoff $K_{max} = 4/R_{MT}$, where R_{MT} is the smallest atomic sphere radius and K_{max} denotes the magnitude of largest k vector in plane wave expansion, while the charge density was Fourier expanded up to $G_{max} = 20$. The muffin-tin radii were assumed to be $0.7a_0$ and $1.1a_0$ for H and N atoms, respectively, where a_0 is the Bohr radius. Self-consistency is obtained using 54 k-points in the irreducible Brillouin zone (IBZ).

3. RESULTS AND DISCUSSION

3.1. Structural and Elastic Properties. NH_4N_3 crystallizes in orthorhombic structure with space group *Pmna* with $a = 8.937$ Å, $b = 3.807$ Å, $c = 8.664$ Å, and $Z = 4$ at ambient conditions.[40] In order to obtain the equilibrium crystal structure, we have performed full structural optimization of NH_4N_3 including lattice parameters and internal coordinates using standard LDA and GGA functionals. We find a difference between calculated and experimental volume of −9.9% with LDA and +3.9% with GGA, and thus, our GGA volume is closer to experiment than LDA volume. This discrepancy between theory and experiment is due to the standard exchange-correlation potentials used in the calculations that do not capture the nature of nonbonded interactions such as hydrogen bonding and van der Waals interactions in molecular solids.[29−31] Therefore, we have performed structural relaxation with the semiempirical approaches known as G06 and TS schemes to include the nonbonded interactions in our calculations. The volume is underestimated by 3.5% using G06, this error is approximately the same as the standard GGA value with opposite sign. However, the TS scheme provides much better volume (293.99 Å^3) 0.3% lesser than the experimental volume (294.78 Å^3), where the deviations in lattice constants a, b, and c are +0.9%, −0.02%, and −1.2%, respectively. The optimized equilibrium crystal structure is in Figure 1. The calculated lattice parameters, volume, and fractional coordinates with standard DFT functionals and semiempirical schemes are presented in Tables 1 and 2, respectively. We have obtained equilibrium bulk modulus, $B_0 =$
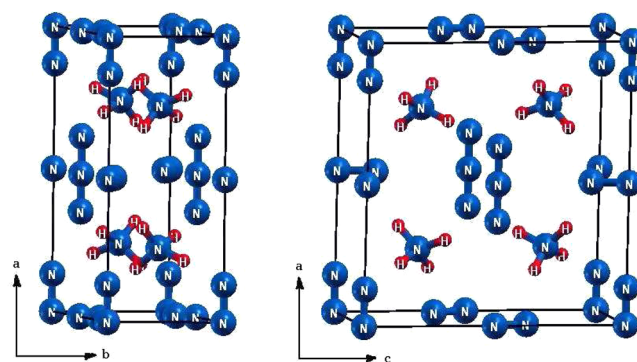

Figure 1. Crystal structure of ammonium azide along (i) $a-b$ and (ii) $a-c$ axes (blue and red colors represent N and H atoms, respectively).

Table 1. Calculated Ground State Lattice Parameters (a, b, and c, in Å) and Volume (V, in Å^3) of NH_4N_3 Using Standard DFT Functionals LDA (CA-PZ), GGA (PBE), and Semiempirical Schemes PBE + G06 and PBE + TS Implemented Thorugh GGA Functional along with Experimental Data

parameter	CA-PZ	PBE	PBE + G06	PBE + TS	experiment[40]
a	8.743	9.094	8.904	9.019	8.937
b	3.631	3.904	3.722	3.806	3.807
c	8.362	8.627	8.585	8.563	8.664
V	265.52	306.36	284.57	293.99	294.78

Table 2. Calculated Fractional Coordinates of NH_4N_3 Using Standard DFT Functionals and Semiempirical Schemes along with Experiment[40]

atom	method	x	y	z
N(M) of N_3	CA-PZ	0.0000	0.0000	0.0000
	PBE	0.0000	0.0000	0.0000
	PBE + G06	0.0000	0.0000	0.0000
	PBE + TS	0.0000	0.0000	0.0000
	exptl	0.0000	0.0000	0.0000
N(M) of N_3	CA-PZ	0.5000	0.0000	0.0000
	PBE	0.5000	0.0000	0.0000
	PBE + G06	0.5000	0.0000	0.0000
	PBE + TS	0.5000	0.0000	0.0000
	exptl	0.5000	0.0000	0.0000
N(T) of N_3	CA-PZ	0.1382	0.0000	0.0000
	PBE	0.1341	0.0000	0.0000
	PBE + G06	0.1366	0.0000	0.0000
	PBE + TS	0.1348	0.0000	0.0000
	exptl	0.1315	0.0000	0.0000
N(T) of N_3	CA-PZ	0.5000	0.1253	0.1338
	PBE	0.5000	0.1435	0.1249
	PBE + G06	0.5000	0.1159	0.1324
	PBE + TS	0.5000	0.1424	0.1270
	exptl	0.5000	0.1103	0.1320
N of NH_4	CA-PZ	0.2500	0.5516	0.2500
	PBE	0.2500	0.5537	0.2500
	PBE + G06	0.2500	0.5474	0.2500
	PBE + TS	0.2500	0.5556	0.2500
	exptl	0.2500	0.5524	0.2500
H(1)	CA-PZ	0.2896	0.7206	0.3450
	PBE	0.2914	0.7104	0.3388
	PBE + G06	0.2902	0.7108	0.3408
	PBE + TS	0.2911	0.7152	0.3403
	exptl	0.2900	0.7310	0.3330
H(2)	CA-PZ	0.3409	0.3842	0.2079
	PBE	0.3349	0.3989	0.2058
	PBE + G06	0.3375	0.3850	0.2073
	PBE + TS	0.3359	0.3977	0.2059
	exptl	0.3230	0.3880	0.1920

26.34 GPa, and its pressure derivative, $B'_0 = 3.6$, by fitting pressure–volume data to the Murnaghan equation of state.[41] The bulk modulus value of NH_4N_3 lies between alkali metal azides (AMAs) and heavy metal azides (HMAs); the reported experimental bulk moduli for AMAs, LiN_3 (19.1 GPa),[42] NaN_3 (16.3 GPa),[43] KN_3 (18.6 GPa),[44] and CsN_3 (18 GPa,)[45] and for HMAs, AgN_3 (39 GPa),[46] and α-$Pb(N_3)_2$ (41 GPa),[43] which indicates that NH_4N_3 is a softer material than HMAs and harder than AMAs. The bulk modulus of NaN_3 and α-$Pb(N_3)_2$ is calculated from their compressibilities.[43] Overall, the present study reveals that the TS scheme works better for molecular crystalline NH_4N_3. Hence, we have used this equilibrium volume to calculate the elastic properties of NH_4N_3.

The elastic constants are fundamental parameters for crystalline solids, which describe stiffness of the solid against externally applied strains. The elastic constants were calculated using volume-conserving strains technique[47] with the PBE + TS scheme. A complete asymmetric crystal behavior can be described by 21 independent elastic constants, due to orthorhombic symmetry of the NH_4N_3 crystal, it has nine independent elastic constants, namely, C_{11}, C_{22}, C_{33}, C_{44}, C_{55}, C_{66}, C_{12}, C_{13}, and C_{23}. The calculated elastic constants are presented in Table 3. The calculated elastic (stiffness) constants are positive and obey the Born's mechanical stability criteria,[48] indicating that NH_4N_3 is mechanically stable at ambient pressure. Eckhardt et al.[49−51] have shown the qualitative association of stiffness constants C_{11}, C_{22}, and C_{33} of crystal with physical phenomena including cleavage planes, patterns in crystal growth, and molecular packing. The strength of interactions between the molecules comprising a molecular crystal has a measurable effect on the macroscopic properties of the solid. Detonation of energetic material can be considered to be a collective property of the material and is highly dependent upon intermolecular interactions, molecular arrangements, and molecular composition. These properties can often be correlated to the strength of the lattice interactions through elastic constants. Since, NH_4N_3 possesses orthorhombic crystal symmetry, the stiffness constants C_{11}, C_{22}, and C_{33} can be directly related to the crystallographic a, b, and c axes, respectively. The observed ordering of stiffness constants in NH_4N_3 is $C_{11} \approx C_{33} > C_{22}$. From the present results, C_{22} is found to have the weakest stiffness constant, which represents a relative weakness of lattice interactions along the crystallographic b axis. The intermolecular interactions are relatively stronger along a and c axes due to the orientation of nitrogen atoms of azide ion in these crystallographic directions (see Figure 1ii). Further, this can be supported by the higher values of stiffness constants C_{11} and C_{33}, when compared to the stiffness constant C_{22}. These results reveal that NH_4N_3 is sensitive to impact along the b crystallographic axis. However, C_{44}, C_{55}, and C_{66} indicate the shear elasticity applied to the two-dimensional rectangular lattice in the (100), (010), and (001) planes. From our calculations, C_{55} is found to be relatively small compared to C_{44} and C_{66}, which is an indication of the soft shear transformation along the (010) plane.

We also derived the polycrystalline properties of NH_4N_3 such as bulk, shear, and Young moduli from the calculated elastic constants using Reuss approximation.[52] The bulk modulus (B) measures resistance of a material against volume

Table 3. Calculated Elastic Constants C_{ij} (in GPa), Bulk Modulus (in GPa), Shear Modulus (in GPa), Density (in g/cm^3), Experimental Density in Parentheses, and Debye Temperature (in K) of NH_4N_3 Using PBE + TS Scheme

C_{11}	C_{22}	C_{33}	C_{44}	C_{55}	C_{66}	C_{12}	C_{13}	C_{23}	B	G	ρ	Θ_D
45.7	35.6	46.3	16.1	10.6	13.3	17.6	19.1	21.9	26.8	12.1	1.357(1.36)[75]	474.5

change under hydrostatic pressure, which indicates the average bond strength of material. The calculated bulk modulus and compressibility are found to be 26.8 and 0.037 GPa^{-1} for NH_4N_3, respectively. The reported[43] compressibilities for different inorganic azides are 0.0615 GPa^{-1} for NaN_3, 0.0541 GPa^{-1} for KN_3, 0.0463 GPa^{-1} for TlN_3, 0.0256 GPa^{-1} for AgN_3,[46] and 0.0244 GPa^{-1} for $\alpha\text{-}Pb(N_3)_2$. The calculated results reveal that NH_4N_3 shows compressibility between AMAs and HMAs. The bulk modulus calculated from the elastic constants is in excellent agreement with the obtained equilibrium bulk modulus from the equation of state. This might be an evidence of reliability and accuracy of our calculated elastic constants for NH_4N_3. The shear modulus (G) represents the resistance to shape change caused by shearing force, which indicates the resistance to change in the bond angle, and it is found to be 12.1 GPa. The Young modulus (E) of a material is defined as the ratio of the linear stress to linear strain, which tells about the stiffness of material. The calculated value 31.6 GPa of NH_4N_3 reveals that the material is stiffer. In general, Poisson's ratio of a material quantifies the stability of crystal against shear strain. If σ is 0.5, no volume change occurs, whereas lower than 0.5 means that the large volume change is associated with elastic deformation.[53] According to our calculation, the σ value is 0.30, which shows that a considerable volume change can be associated with the deformation in NH_4N_3. According to Pugh's criterion,[54] the B/G ratio less than (greater than) the critical value of 1.75 indicates the brittle (ductile) nature of materials. In the present case, it is found to be 2.2, which implies that NH_4N_3 is a ductile material. This is also confirmed by the Cauchy's pressure ($C_{12}-C_{44}$), the negative and positive values of Cauchy's pressure indicate the brittle and ductile nature of materials, respectively.[55] A positive value of Cauchy's pressure indicating that NH_4N_3 has ductile nature, as commonly expected for ionic insulators. Further, we also estimated the Debye temperature Θ_D, which is a fundamental quantity that determines the thermal characteristics of material. A high value of Θ_D implies higher thermal conductivity. At low temperatures Θ_D, can be estimated from the average wave velocities (v_m) of longitudinal (v_l) and transverse (v_t) modes as mentioned in refs 53 and 56. The calculated values of v_l, v_t, and v_m are 5.62, 2.99, and 3.34 km/s respectively, which yields a Θ_D of 474.5 K (see Table 3). This is the first qualitative prediction of elastic properties of NH_4N_3 that still awaits experimental confirmation.

3.2. Electronic Structure and Chemical Bonding.
Electronic structure of inorganic azides have been investigated by X-ray electron spectroscopy[57] to understand the chemical bonding. This study reveals that the ionic character intensifies in AMAs as follows, $LiN_3 < NaN_3 < KN_3 < RbN_3 < CsN_3$; this is in very good agreement with the recently reported[45] trend for the AMAs, while being the same in HMAs, (AgN_3, CuN_3, $Cu(N_3)_2$, $Hg(N_3)_2$, $Hg_2(N_3)_2$) < (TlN_3, $\alpha\text{-}Pb(N_3)_2$) < $Cd(N_3)_2$, which indicates that AMAs are more ionic than HMAs, implying that AMAs are relatively more stable than HMAs. In order to understand the relative stability of NH_4N_3 when compared to the mentioned inorganic azides, it is necessary to know the electronic structure and chemical bonding in NH_4N_3. The electronic structure determines the fundamental physical and chemical properties such as initiation, decomposition, and detonation of an energetic material. Electronic band gap is an important property for energetic materials, which can be used to predict the relative stability and sensitivity,[58] but the standard DFT functionals always under-

estimate the band gap approximately 50% when compared to experiments. Hence, we need more accurate methods such as GW approximation[59,60] in order to get a reliable value for energy gap. Recent studies[38,61−64] show that the TB-mBJ functional provides fairly accurate energy gaps for semiconductors and insulators, and also this method is computationally less expensive when compared to the former method. Therefore, we have used this TB-mBJ functional to calculate electronic structure and optical properties of NH_4N_3 at ambient pressure. Previous theoretical studies[58,65−67] revealed the relationship between band gap and impact sensitivity for the metal azides and CHNO based energetic materials within the framework of periodic DFT calculations. Further, Kuklja et al.[68,69] investigated the excitonic mechanism of detonation initiation in explosives and clarified that pressure inside the impact wavefront reduces the band gap. It can be expected that the smaller the band gap, the easier the electron transfers from valence band to conduction band; thus, the energetic system becomes more and more sensitive to external stimuli such as light, heat, friction, and impact. The calculated band structure of NH_4N_3 along high symmetry directions is as follows, Γ-point at 5.08 eV; Z, T, U, R-points at 5.29 eV; Y-point at 5.21 eV, and S, X-points at 5.24 eV in the first Brillouin zone as shown in Figure 2. The top of the valence band and the bottom of the
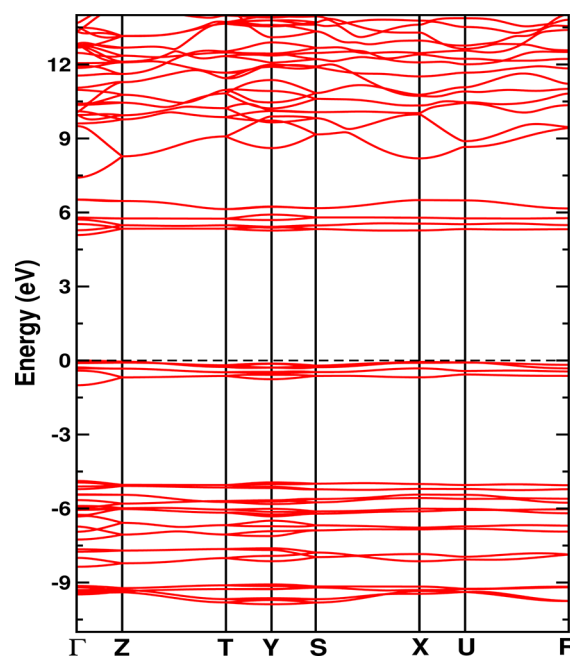

Figure 2. Calculated band structure of NH_4N_3 along high symmetry directions in the Brillouin zone Γ (0.0, 0.0, 0.0) → Z (0.0, 0.0, 0.5) → T (0.0 0.5, 0.5) → Y (0.0 0.5 0.0) → S (0.5, 0.5, 0.0) → X (0.5, 0.0, 0.0) → U (0.5, 0.0, 0.5) → R (0.5, 0.5, 0.5) using the TB-mBJ functional at the experimental crystal structure.

conduction band occur along the $\Gamma-\Gamma$ direction, indicating that this material is a direct band gap insulator with a minimum separation of 5.08 eV. The corresponding band gap value using GGA-PBE functional is 4.10 eV. Experimental band gap value when available could be compared to our theoretical band gap.

In order to explain the chemical bonding in NH_4N_3, we have calculated total and partial density of states (PDOS); see Figure 3. The conduction band is mainly dominated by 2p states of nitrogen atoms (N(T), N(M), N of NH_4) and 1s states of

16913

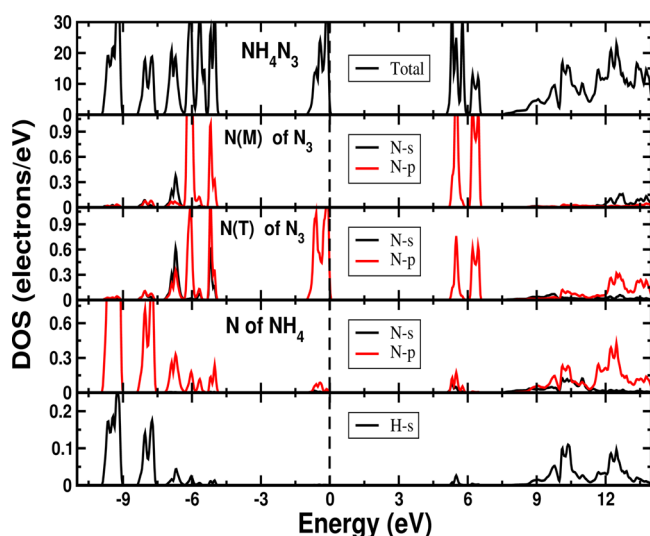dx.doi.org/10.1021/jp3054839 | J. Phys. Chem. C 2012, 116, 16910−16917

Figure 3. Calculated total and PDOS of NH_4N_3 using the TB-mBJ functional at the experimental crystal structure. N(T) and N(M) represent terminal and middle nitrogen atoms of azide anion, respectively.

hydrogen (H) atom. The top of valence band is completely dominated by 2p states of terminal nitrogen N(T) of azide ion, which implies that these states might be responsible for initiation of the decomposition process in NH_4N_3. The relatively less contribution from 2p states of NH_4 ion, when compared to azide ion in the valence band region up to −4.5 eV from Fermi level, indicates a degree of nondirectional (ionic) bonding between ammonium (NH_4^+) and azide (N_3^-)

ions. There is considerable overlap between 2p states of terminal N(T) and middle N(M) nitrogens of azide ion as well as 2p states of nitrogen from NH_4 and s states of nitrogen atoms of azide ion in the energy range from −7.5 to −5 eV. Similarly, in the energy range from −10.5 to −7.5 eV, 2p states of nitrogen atom from NH_4 overlap with 1s states of the hydrogen atom. This does suggest that there is hybridization between N(T)−N(M) of azide ion and H−N of NH_4, implying directional (covalent) bonding in N−N (nitrogen atoms of azide ion) and N−H bonds. The Pauling scale has been used as a measure of the attraction ability of an atom for electrons in a covalent bond.[70] The difference in Pauling electronegativities of nitrogen (3.0) and hydrogen (2.1) is used to predict the nature of the N−H bond in ammonium ion. The electronegativity difference is 0.9, which points to a polar covalent bond character of N−H bond. In ammonium ion, the unit positive charge of the complex might be residing more on the nitrogen atom, as a consequence of polar covalent character of the N−H bond. This can be clearly understood from the electronic charge density contours along (200), (101), and (010) planes of NH_4N_3 crystal as shown in Figure 4. The charge density along N(T)−N(M) is pronounced due to the hybridization between terminal and middle nitrogen of azide anion, suggesting directional bonding in azide ion. However, there is very less charge sharing between NH_4^+ and N_3^- (see Figure 3) ions indicating that ionic bonding is predominant in NH_4N_3. The nature of bonding in NH_4N_3 is interpreted through bulk modulus, Colton et al. determined ionic character (in %) for the AMAs and HMAs and found that AMAs are ionic solids, while the HMAs are covalent solids.[57] Also, the bulk moduli of AMAs are lower when compared to HMAs (see section 3.1), which reveals that the covalent azides have higher bulk modulus
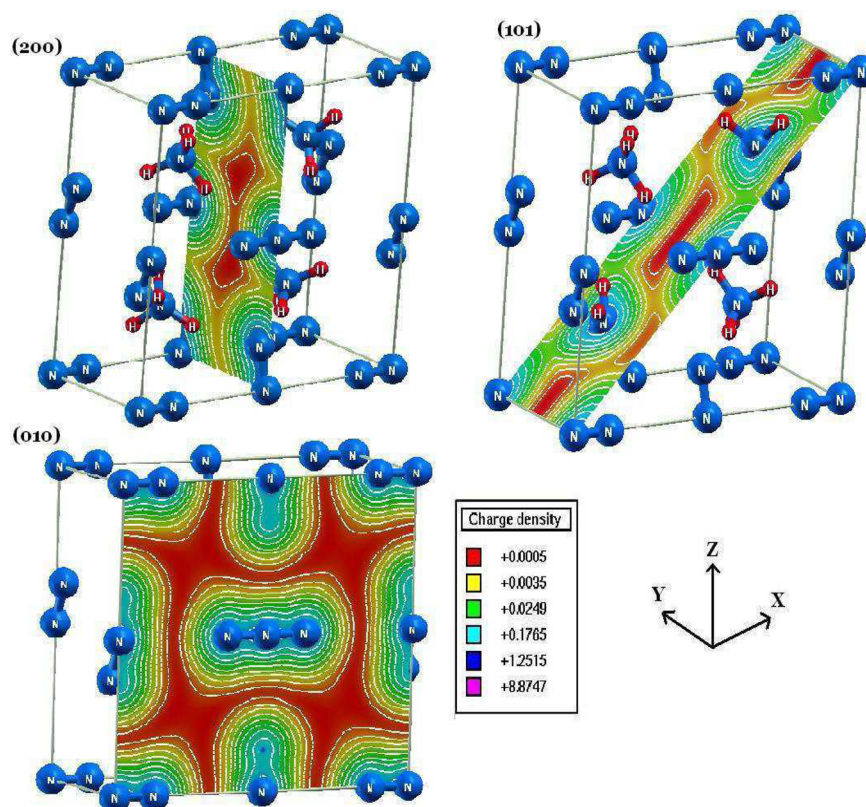

Figure 4. Calculated electronic charge densities of NH_4N_3 in (200), (101), and (010) planes.

than ionic azides due to strong directional bonding. The bulk modulus of NH_4N_3 is found to be in the middle of the AMAs and HMAs. Therefore, we confirmed from the calculated electronic band structure, DOS, charge density distributions, and bulk modulus that NH_4N_3 exhibits predominantly ionic bonding along with partial covalent nature from the N−H and N−N bonds of NH_4^+ and N_3^- ions, respectively.

3.3. Optical Properties. The linear response of a system to electromagnetic radiation can be described by means of the dielectric function. In general, there are two contributions to dielectric function, namely, intra- and interband transitions. The intraband transitions occur only in metals. Further, the interband transitions are classified into direct and indirect transitions. The indirect interband transitions arise from scattering of phonons, which are neglected in our calculations because their contribution is negligible to the dielectric function when compared to direct interband transitions. The contribution of direct interband transitions to the imaginary $\epsilon_2(\omega)$ part of the dielectric function in the random phase approximation[71] without local field effects can be calculated by summing all the possible transitions between the occupied and unoccupied states for a set of k-vectors over the Brillouin zone. The real $\epsilon_1(\omega)$ part of dielectric function can be derived from the imaginary $\epsilon_2(\omega)$ part of dielectric function by using Kramers−Kronig relationship.[72]

The linear optical properties of NH_4N_3 have been calculated using TB-mBJ electronic structure with denser k-mesh of 735 k-points in the IBZ. NH_4N_3 crystallizes in the orthorhombic $Pmna$ space group; this symmetry has three independent components of dielectric function. Hence, the real and imaginary part of dielectric function are determined as a function of photon energy along three crystallographic ([100], [010], and [001]) directions as shown in Figure 5. The imaginary part of the dielectric function $\epsilon_2(\omega)$ has three prominent peaks due to interband transitions between the valence band maximum (VBM) and conduction band minimum (CBM) along three crystallographic axes. The peaks in $\epsilon_2(\omega)$ (see Figure 5b) are divided into three energy regions, named as A, 5−7.5 eV; B, 11.5−13.5 eV; and C, 17.5−
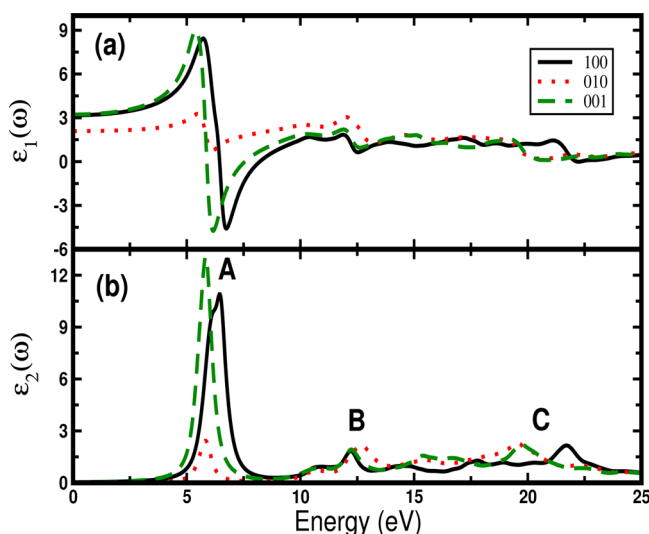
23.5 eV. The peaks in the region A are due to interband transitions between 2p states of terminal nitrogen N(T) of azide ion to s states of H/N of NH_4, while the peaks in region B as result of transitions between N-2p of NH_4 to H-1s states. Finally, the peaks in region C originate from H-1s to N-2p states of NH_4 and vice versa. It should be noted that most of the optical transitions are mainly from 2p(N) → 1s(H) states. The static real part of dielectric function $\epsilon_1(\omega)$ along three crystallographic directions is found to be 3.18 (along [100]), 2.09 (along [010]), and 3.22 (along [001]). Further, we have derived the four important optical constants absorption spectra $\alpha(\omega)$, refractive index $n(\omega)$, reflectivity $R(\omega)$, and loss function $L(\omega)$ of NH_4N_3 as a function of photon energy from the calculated real and imaginary parts of dielectric function using the formulations given in the ref 72. They have been displayed in Figure 6. As shown from Figure 6a, the absorption starts
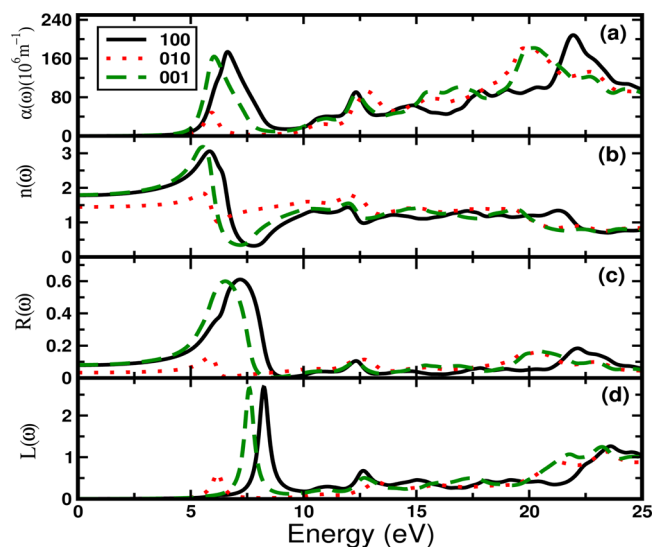

Figure 6. Calculated absorption spectra $\alpha(\omega)$, refractive index $n(\omega)$, reflectivity $R(\omega)$, and loss function $L(\omega)$ of NH_4N_3 as a function of photon energy at ambient conditions. Black solid line (along [100]), red dotted line (along [010]), and green thick dotted line (along [001]).

from 5.08 eV, which is a fundamental energy gap between VBM and CBM known as fundamental absorption edge for NH_4N_3. The first absorption peaks along three crystallographic directions [100], [010], and [001] are at 6.64, 5.94, and 6.03 eV, and the corresponding absorption coefficients are 1.7×10^8 m^{-1}, 4.7×10^7 m^{-1}, and 1.6×10^8 m^{-1}, respectively. This result reveals that NH_4N_3 decomposes under the action of UV light. The absorption takes place from 5.08 (fundamental absorption edge) to 25 eV, and then, it decreases in the high energy region because the crystal becomes transparent above 25 eV.

The calculated static refractive index of NH_4N_3 along the crystallographic axes is 1.78 (along [100]), 1.45 (along [010]), and 1.80 (along [001]). The distinct static refractive index values in each crystallographic direction indicates that NH_4N_3 is a optically anisotropic crystal (see Figure 6b). The electron energy-loss function $L(\omega)$ describes the energy loss of a fast electron traversing in a material. The peaks in the $L(\omega)$ spectra represent the characteristics associated with the plasma resonance, and the corresponding frequency is the so-called plasma frequency, above which the material is a dielectric ($\epsilon_1(\omega) > 0$), and below which the material behaves like a

Figure 5. Real $\epsilon_1(\omega)$ and imaginary $\epsilon_2(\omega)$ parts of dielectric function of NH_4N_3 along three crystallographic axes as a function of photon energy at ambient conditions. Black solid line (along [100]), red dotted line (along [010]), and green thick dotted line (along [001]).

metallic compound ($\epsilon_1(\omega) < 0$). As illustrated in Figure 6d, the prominent peaks in $L(\omega)$ correspond to the trailing edges in the reflection spectra (see Figure 6c) observed at 8.2 eV (along [100]), 6.1 eV (along [010]), and 7.6 eV (along [001]) directions and about 23.5 eV in all the three directions corresponding to abrupt reduction in the reflection spectra $R(\omega)$.

3.4. Detonation Properties. For an explosive, detonation velocity (D) and detonation pressure (P) are the most important factors to evaluate its performance. The Kamlet–Jacobs equations[73,74] based on the reported density and heat of formation (HOF) were chosen for the prediction of detonation performance. Values for D (in km/s) and P (in GPa) were calculated according to the following equations:

$$D = 1.01(NM^{0.5}Q^{0.5})^{0.5}(1 + 1.30\rho_0) \quad \text{and}$$

$$P = 1.55\rho_0{}^2NM^{0.5}Q^{0.5}$$

In the above equations, N is moles of gaseous detonation products per gram of explosives, M is average molecular weights of gaseous products, Q is chemical energy of detonation (kJ/mol) defined as the difference of the HOFs between products and reactants, and ρ_0 is the density of explosive (g/cm^3). We calculated the detonation velocity and pressure using calculated density (1.357 g/cm^3) and reported HOF (112.8 kJ/mol),[75,76] and the corresponding values are found to be 6.45 km/s and 15.16 GPa, respectively.

4. CONCLUSIONS

In the present study, first-principles calculations were performed to investigate the structural, elastic, electronic, and optical properties of NH_4N_3. The standard DFT functionals such as LDA and GGA are unable to account for the nonbonded dispersive forces in NH_4N_3 (see Table 1). The calculated ground state properties using TS scheme are in excellent agreement with the experiment. Hence, we have used this scheme to calculate the elastic constants of NH_4N_3, and it is found to be mechanically stable. The observed ordering of the elastic constants is $C_{11} \approx C_{33} > C_{22}$, implying that NH_4N_3 is sensitive along the b axis due to weak intermolecular interactions between the atoms along this axis. We have derived the polycrystalline properties such as bulk modulus, shear modulus, density, and Debye temperature from the calculated elastic constants. Finally, our PW-PP calculations confirm that the semiempirical schemes (TS and G06) can successfully treat the van der Waals interactions in NH_4N_3. The TB-mBJ electronic structure shows that NH_4N_3 is a direct band gap insulator with an energy gap of 5.08 eV. The calculated PDOS and charge density contours show that strong ionic and weak covalent bonding nature in NH_4N_3. This is also confirmed by the obtained equilibrium bulk modulus of NH_4N_3 by comparing with bulk moduli of various inorganic azides. The calculated static refractive index and dielectric constants along the three different crystallographic axes indicate a strong anisotropy in NH_4N_3. Also, the absorption spectra reveal that NH_4N_3 is sensitive to UV light. Finally, the detonation velocity and detonation pressure are calculated using Kamlet–Jacobs equations from experimental heat of formation and calculated density. NH_4N_3 shows moderate performance, and the predicted detonation velocity and detonation pressure are 6.45 km/s and 15.16 GPa, respectively.

■ AUTHOR INFORMATION

Corresponding Author
*E-mail: gvsp@uohyd.ernet.in.

Notes
The authors declare no competing financial interest.

■ REFERENCES

(1) Fair, H. D.; Walker, R. F. *Energetic Materials*; Plenum Press: New York, 1977; Vol. *1*.
(2) Bowden, F. P.; Yoffe, A. D. *Fast Reactions in Solids*; Butterworth: London, U.K., 1958.
(3) Eremets, M. I.; Hemley, R. J.; Mao, H. K.; Gregoryanz, E. *Nature* **2001**, *411*, 170−174.
(4) Eremets, M. I.; Gavriliuk, A. G.; Trojan, I. A.; Dzivenko, D. A.; Boehler, R. *Nat. Mater.* **2004**, *3*, 558−563.
(5) Eremets, M. I.; Popov, M. Y.; Trojan, I. A.; Denisov, V. N.; Boehler, R.; Hemley, R. J. *J. Chem. Phys.* **2004**, 10618−10623.
(6) Medvedev, S. A.; Eremets, M. I.; Evers, J.; Klapotke, T. M.; Palasyuk, T.; Trojan, I. A. *Chem. Phys.* **2011**, *386*, 41−44.
(7) Medvedev, S. A.; Palasyuk, T.; Trojan, I. A.; Naumov, P. G.; Evers, J.; Klapotke, T. M.; Eremets, M. I. *Vib. Spectrosc.* **2012**, *58*, 188−192.
(8) Prince, E.; Choi, C. S. *Acta Crystallogr., Sect. B: Struct. Sci.* **1978**, *34*, 2606−2608.
(9) Curtius, T. *Ber. Deutsch. Chem. Gesellschaft* **1890**, *23*, 3023−3033.
(10) Eslami, A.; Hosseini, S. G.; Shariaty, S. H. M. *Powder Technol.* **2011**, *208*, 137−143.
(11) Ng, W. L.; Field, J. E. *Thermochim. Acta* **1985**, *84*, 133−140.
(12) Evers, J.; Gobel, M.; Krumm, B.; Martin, F.; Medvedyev, S.; Oehlinger, G.; Steemann, F. X.; Troyan, I.; Klapotke, T. M.; Eremets, M. I. *J. Am. Chem. Soc.* **2011**, *133*, 12100−12105.
(13) Yakovleva, G. S.; Kurgangalina, R. K.; Stestik, L. N. *Goreniya Vzryva* **1977**, *13*, 473−475.
(14) Masaaki, S.; Takehiko, S.; Tadamasa, H.; Ikuo, H. *Japan Kokai* **1974**, *74*, 08475.
(15) Maycock, J. N.; Pai Verneker, V. R. *J. Spacecr. Rockets* **1969**, *6*, 336−337.
(16) Sarner, S. R. *Propellant Chemistry*; Van Nostrand Reinhold: New York, 1966.
(17) Hu, A.; Zhang, F. *J. Phys.: Condens. Matter* **2011**, *23*, 022203.
(18) Yakovleva, G. S.; Kurgangalina, R. K.; Stesik, L. N. *Combust. Explos. Shock* **1997**, *13*, 405−407.
(19) Finch, A.; Gardner, P. J.; Head, A. J.; Xiaoping, W. *J. Chem. Thermodyn.* **1990**, *22*, 301−305.
(20) Payne, M. C.; Teter, M. P.; Allen, D. C.; Arias, T. A.; Joannopoulos, J. D. *Rev. Mod. Phys.* **1992**, *64*, 1045−1097.
(21) Milman, V.; Winkler, B.; White, J. A.; Packard, C. J.; Payne, M. C.; Akhmatskaya, E. V.; Nobes, R. H. *Int. J. Quantum Chem.* **2000**, *77*, 895−910.
(22) Segall, M. D.; lidan, P. L. D.; Probert, M. J.; Pickard, C. J.; Hasnip, P. J.; Clark, S. J.; Payne, M. C. *J. Phys: Condens. Matter* **2002**, *14*, 271−280.
(23) Hohenberg, P.; Kohn, W. *Phys. Rev. B* **1964**, *136*, 384−389.
(24) Kohn, W.; Sham, L. J. *Phys. Rev. A* **1965**, *140*, 1133−1138.
(25) Vanderbilt, D. *Phys. Rev. B* **1990**, *41*, 7892−7895.
(26) Ceperley, D. M.; Alder, B. J. *Phys. Rev. Lett.* **1980**, *45*, 566−569.
(27) Perdew, J. P.; Zunger, A. *Phys. Rev. B* **1981**, *23*, 5048−5079.

(28) Perdew, J. P.; Burke, S.; Ernzerhof, M. *Phys. Rev. Lett.* **1996**, *77*, 3865−3868.

(29) Santra, B.; Klimes, J.; Alfe, D.; Tktchenko, A.; Slater, B.; Michaelides, A.; Car, R.; Scheffler, M. *Phys. Rev. Lett.* **2011**, *107*, 185701.

(30) Lu, D.; Li, Y.; Rocca, D.; Galli, G. *Phys. Rev. Lett.* **2009**, *102*, 206411.

(31) Dion, M.; Rydberg, H.; Schroder, E.; Langreth, D. C.; Lundqvist, B. I. *Phys. Rev. Lett.* **2004**, *92*, 246401.

(32) Grimme, S. *J. Comput. Chem.* **2006**, *27*, 1787−1799.

(33) Tkatchenko, A.; Scheffler, M. *Phys. Rev. Lett.* **2009**, *102*, 073005.

(34) Fischer, T. H.; Almlof, J. *J. Phys. Chem.* **1992**, *96*, 9768−9774.

(35) Monkhorst, H. J.; Pack, J. D. *Phys. Rev. B* **1976**, *13*, 5188−5192.

(36) Nieminen, R. M. *Modell. Simul. Mater. Sci. Eng.* **2009**, *17*, 084001.

(37) Sham, L. J.; Schluter, M. *Phys. Rev. Lett.* **1983**, *51*, 1888.

(38) Tran, F.; Blaha, P. *Phys. Rev. Lett.* **2009**, *102*, 226401.

(39) Blaha, P.; Schwarz, K.; Madsen, G. K. H.; Kvasnicka, D.; Luitz, J. *WIEN2K, an Augmented Plane Wave + Local Orbitals Program for Calculating Crystal Properties*; Karlheinz Schwarz Technische Universitat: Wien, Austria, 2001.

(40) De Amorim, H. S.; do Amaral, M. R., Jr.; Pattison, P.; Ludka, I. P.; Mendes, J. C. *J. Mex. Chem. Soc.* **2002**, *46*, 313−319.

(41) Murnaghan, F. D. *Proc. Natl. Acad. Sci. U.S.A.* **1944**, *30*, 244−247.

(42) Medevdev, S. A.; Trojan, I. A.; Eremets, M. I.; Palasyuk, T.; Klapotke, T. M.; Evers, J. *J. Phys.: Condens. Matter* **2009**, *21*, 195404.

(43) Weir, C. E.; Block, S.; Piermarini, G. J. *J. Chem. Phys.* **1970**, *53*, 4265−4269.

(44) Ji, C.; Zhang, F.; Hou, D.; Zhu, H.; Wu, J.; Chyu, M. C.; Levitas, V. I.; Ma, Y. *J. Phys. Chem. Solids* **2011**, *72*, 736−739.

(45) Hou, D.; Zhang, F.; Ji, C.; Hannon, T.; Zhu, H.; Wu, J.; Ma, Y. *Phys. Rev. B* **2011**, *84*, 064127.

(46) Hou, D.; Zhang, F.; Ji, C.; Hannon, T.; Zhu, H.; Wu, J.; Levitas, V. I.; Ma, Y. *J. Appl. Phys.* **2011**, *110*, 023524.

(47) Mehl, M. J.; Osburn, J. E.; Papaconstantopoulos, D. A.; Klein, B. M. *Phys. Rev.B* **1990**, *41*, 10311−10323.

(48) Born, M.; Huang, K. *Dynamical Theory of Crystal Lattices*; Oxford University Press: Oxford, U.K., 1998.

(49) Haycraft, J. J.; Stevens, L. L.; Eckhardt, C. J. *J. Chem. Phys.* **2006**, *124*, 024712.

(50) Stevens, L. L.; Eckhardt, C. J. *J. Chem. Phys.* **2005**, *122*, 174701.

(51) Eckhardt, C. J. *J. Chem. Phys.* **2009**, *131*, 214501.

(52) Reuss, A.; Angew, Z. *Math. Phys.* **1929**, *9*, 49.

(53) Ravindran, P.; Fast, L.; Korzhavyi, P. A.; Johansson, B. *J. Appl. Phys.* **1998**, *84*, 4891−4904.

(54) Pugh, S. F. *Philos. Mag.* **1954**, *45*, 823−843.

(55) Pettifor, D. G. *Mater. Sci. Technol.* **1992**, *8*, 345−349.

(56) Anderson, O. L. *J. Phys. Chem. Solids* **1963**, *24*, 909−917.

(57) Colton, R. J.; Rabalais, J. W. *J. Chem. Phys.* **1976**, *64*, 3481−3486.

(58) Zhu, W. H.; Xiao, H. M. *Struct. Chem.* **2010**, *21*, 847−854.

(59) Hedin, L. *Phys. Rev.* **1965**, *139*, A796−A823.

(60) Hedin, L.; Lundquist, S. *Solid State Physics*; Academic Press: NewYork, 1969; Vol. *23*, p 1.

(61) Koller, D.; Tran, F.; Blaha, P. *Phys. Rev. B* **2012**, *85*, 155109.

(62) Koller, D.; Tran, F.; Blaha, P. *Phys. Rev. B* **2011**, *83*, 195134.

(63) Dixit, H.; Saniz, R.; Cottenier, S.; Lamoen, D.; Partoens, B. *J. Phys.: Condens. Matter* **2012**, *24*, 205503.

(64) Singh, D. J. *Phys. Rev. B* **2010**, *82*, 205102.

(65) Zhu, W. H.; Xiao, H. M. *J. Comput. Chem.* **2008**, *29*, 176−184.

(66) Zhu, W. H.; Xiao, J. J.; Ji, G. F.; Zhao, F.; Xiao, H. M. *J. Phys. Chem. B* **2007**, *111*, 12715.

(67) Xu, X. J.; Zhu, W. H.; Xiao, H. M. *J. Phys. Chem. B* **2007**, *111*, 2090−2097.

(68) Kuklja, M. M.; Stefanovich, E. V.; Kunz, A. B. *J. Chem. Phys.* **2000**, *112*, 3417−3423.

(69) Kuklja, M. M.; Kunz, A. B. *J. Appl. Phys.* **2000**, *87*, 2215−2218.

(70) Pauling, L. *The Nature of the Chemical Bond*, 3rd ed.; Cornell University Press: Ithaca, NY, 1960.

(71) Ehrenreich, H.; Cohen, M. H. *Phys. Rev.* **1959**, *115*, 786−790.

(72) Fox, M. *Optical Properties of Solids*; Oxford University Press: New York, 2001.

(73) Kamlet, M. J.; Jacobs, S. J. *J. Chem. Phys.* **1968**, *48*, 23−35.

(74) Kamlet, M. J.; Ablard, J. E. *J. Chem. Phys.* **1968**, *48*, 36−42.

(75) Williams, L. O. US Patent 5,081,930, 1992.

(76) Gray, P.; Waddington, T. C. *Proc. R. Soc. Lond., A* **1956**, *235*, 481−495.

16917

dx.doi.org/10.1021/jp3054839 | *J. Phys. Chem. C* 2012, 116, 16910−16917